Re-Entry Behavior of Zirconium Hydride-Uranium Fuel Elements

FRED E. LITTMAN*
Stanford Research Institute, Menlo Park, Calif.

An important aspect of the utilization of nuclear auxiliary power systems in aerospace vehicles is the safe disposal of the radioactive materials they contain. In this study the behavior of zirconium hydride-uranium fuel elements was investigated by subjecting them to stagnation pressure and heat-flux conditions for selected trajectories, using an arc image furnace. The results suggest that zirconium hydride-uranium is highly resistant to the conditions encountered on re-entry from a decaying orbit, making it unlikely that adequate dispersal of the fuel-element material can be achieved.

Introduction

WHEN nuclear-powered energy sources are carried in aerospace vehicles, it will be necessary to dispose of them or recover them at the ends of their projected flights. Incineration during their re-entry into earth's atmosphere has been considered as a practical means of safe disposal, provided that this process results in particles small enough to remain suspended for a long time or to become sufficiently dispersed.

The present program was devised specifically to obtain information regarding the burnup of nuclear auxiliary power systems of the NAPS-2 type, which contain a miniaturized nuclear reactor in which zirconium-uranium hydride fuel elements are used. These fuel elements (and the fission product inventory they contain at the end of the projected life) constitute the main hazard of radioactive contamination.

This study was an experimental investigation of the fate of a zirconium-uranium hydride fuel element subjected to simulated re-entry conditions of stagnation heating and pressures. Its purpose was to determine, insofar as possible with available laboratory apparatus and reasonable effort, the melting and oxidation behavior of this material, to obtain information on the particle size of the resulting products of combustion, and to help establish a generalized model of the behavior of fuel rod material under re-entry conditions.

It should be emphasized that only two parameters were simulated in this work: stagnation heat flow and stagnation pressure. No attempt was made to simulate dynamic gas flow. It was felt, however, that these limitations did not introduce major uncertainties for the following reasons: 1) the shear forces created by dynamic conditions are small compared to the tensile strength of an oxide layer and, therefore, are not likely to remove it; and 2) the oxidation reactions of zirconium are only slightly pressure dependent, which reduces the importance of the increased oxygen supply provided by dynamic (over static) conditions.

Since the statement of the problem required a breakup of the fuel rod above 100,000 ft to assure freedom from local ground contamination, reactions in the lower atmosphere were not considered. Similarly, the effect of cladding was neglected, since this material melts at a much lower temperature and has a lower heat content than an equivalent thickness of zirconium-uranium alloy.

Received April 22, 1963; revision received January 21, 1964. The work described in this paper was sponsored by Air Force Special Weapons Center, Air Force Systems Command, Kirtland Air Force Base, New Mexico, under Contract AF 29(601)-4954, Project 1831, Task 183101. Many people have contributed to this study, and this report is the sum total of these efforts. In particular, Arthur Reed, who operated the arc image furnace, and Dante Petro, who spent many hours developing satisfactory metallographic techniques, are largely responsible for the success of this study. The importance of the technical meetings of the contractors of Project 1831, who, under the auspices of the AFSWC Project Officers, guided the over-all direction of these studies, can hardly be overestimated and is gratefully acknowledged.

* Senior Research Chemist; presently Senior Research Scientist, Astropower Laboratory, Douglas Aircraft Corporation, Inc., Newport Beach, Calif.

Experimental Approach: Methods and Equipment

This study was part of a cooperative effort of a number of contractors under the direction of Air Force Special Weapons Center. Thus, the conditions to be examined were decided upon by mutual agreement of the investigators involved and the model trajectories calculated by one of them.†

It was decided to investigate conditions encountered by an object re-entering in a polar orbit starting at the north pole, having a velocity of 25,680 fps, a zero entering angle, and a ballistic parameter W/C_DA of 20 (rod normal to trajectory) and 300 (rod axial) lb/ft^2. It was further assumed that, for each ballistic parameter, the ejection of the fuel rods would occur at each of these altitudes: 400, 300, 250, 200, 150, or 100 kft; for convenience, the trajectories were designated the *a* and *b* series according to the following scheme (Table 1). In the heat-transfer calculations, a cold-wall temperature of 500°R was assumed. The 5*a*, 4*b*, and 5*b* trajectories were not included in the experimental approach, because in those trajectories the total integrated heat content drops below the amount of heat required to melt a 1.25-in. fuel element (of the order of 2400 Btu).[1]

For experimental purposes, both the flux and the pressure values were averaged over periods of time ranging from 300–20 sec, depending on the slope of the curves, as shown in the accompanying diagrams. The actual flux used was increased by 50% in most runs to compensate for two factors: the experimental conditions, which permitted the heating of only one face of the sample while at the same time it was radiating from five sides; and, offsetting this to some extent, the reduction of stagnation-point flux to average flux by a factor of 3 because of the tumbling of the rod. Assuming that the sample is at uniform temperature and that all heat loss

Table 1 Trajectory designations

Ejection ht, kft	Trajectory $W/C_DA = 20$	Trajectory $W/C_DA = 300$
400	*a*	*b*
300	1*a*	1*b*
250	2*a*	2*b*
200	3*a*	3*b*
150	4*a*	4*b*
100	5*a*	5*b*

† General Dynamics/Astronautics, San Diego, Calif.

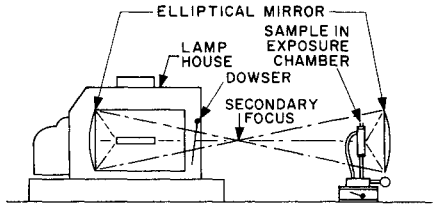

Fig. 1 Schematic diagram of arc image furnace.

is by radiation, the requirement of heat input by the arc image furnace equal to that by stagnation heating is given by the relation

$$\epsilon \dot{q}_i A_i = \tfrac{1}{3} q_s A_t$$

where ϵ is the emissivity, $\dot{q}$ the heat flux, A the area, and the subscripts i, s, and t refer to arc image input, stagnation, and total. Assuming $\epsilon = 0.8$ and our particular wedge-shaped sample ($A_i/A_t = 0.275$), we find $q_i = 1.5\ \dot{q}_s$, requiring a 50% increase in incident flux.

Arc Image Furnace

The major piece of equipment used is an arc image furnace equipped with 14-in. elliptical mirror. This apparatus, a lineal descendant of the mirror system used by Archimedes in 212 B.C. to burn the ships of the invading Roman navy at Syracuse, consists of a carbon arc system as a source of energy and a pair of elliptical mirrors whose function is to collect and transfer this energy to another plane, the furnace area. Flux densities of the order of 900 Btu/ft²-sec can easily be obtained by commercial equipment and maintained for 20–30 min, the lifetime of a carbon electrode. These flux densities correspond to a blackbody temperature of over 5000°R. Control of the flux density can best be achieved by decreasing the area of the subtended angle of the secondary mirror by means of continuous or step diaphragms.

The sample rested on a zirconia column that was contained in a borosilicate glass exposure chamber. For experiments at less than atmospheric pressure, a thin-walled, spherical container was used which did not absorb a measurable amount of radiant energy. For high-pressure experiments, a thick-walled glass container was used which reduced the incident energy by about 20%. Figure 1 shows a schematic diagram of the equipment; Fig. 2, a close-up of a typical sample.

The furnace was calibrated with a radiometer developed by the Naval Defense Radiological Laboratories. This meter consists essentially of a small, blackened, silver disk

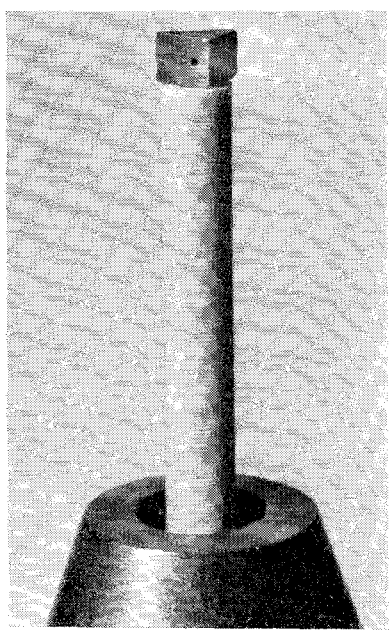

Fig. 2 Typical sample.

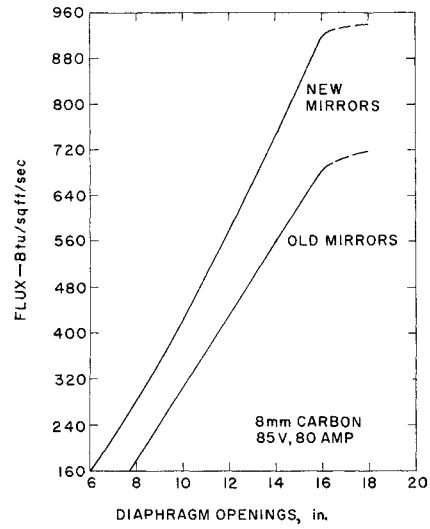

Fig. 3 Calibration curve for arc image furnace.

to which a thermocouple is connected. The disk is embedded in a water-cooled copper block, which constitutes an infinite heat sink. The temperature reached by the black target is directly proportional to the heat input. Figure 3 shows the results obtained by using this meter for two different sets of mirrors. The new mirrors were used for all experiments requiring high flux levels.

Pressures were measured with an assortment of gages, depending on the desired range. A McLeod gage was used for pressures up to 0.1 in., a manometer for pressures up to atmospheric pressure, and a Bourdon gage for higher pressures. Pressure, as well as flux, was changed stepwise, as indicated on the diagrams representing the several trajectories.

Optical measurement of temperatures proved to be quite difficult, because reflection of the arc on the surface of the sample resulted in high readings. The problem was eventually solved by using a Micro Optical Pyrometer, which was focused on a hole 0.025 in. in diameter and 0.150 in. deep, drilled into the side of the sample. The hole can be seen clearly in Fig. 2. Drilling holes into the hydrided samples was exceedingly difficult, but it was accomplished eventually with a supersonic drill. The temperature readings thus obtained closely approximate blackbody temperatures, since it can be shown that an apparent emissivity of 0.99 results with a hole having a depth of 2.6 diam and a surface emissivity of 0.75.[2]

Experimental Procedures

Except for a few early runs in which cubic samples were used, the samples were wedge shaped, approximately $\frac{3}{16}$ in. on edge. Two types of material were used: zirconium-10% uranium alloy, and hydrided material of the same starting composition, containing about 1.9 atoms of hydrogen per atom of zirconium. The uranium was not enriched, so no special precautions were required in handling it. Typical photomicrographs of the starting material are shown in Figs. 4

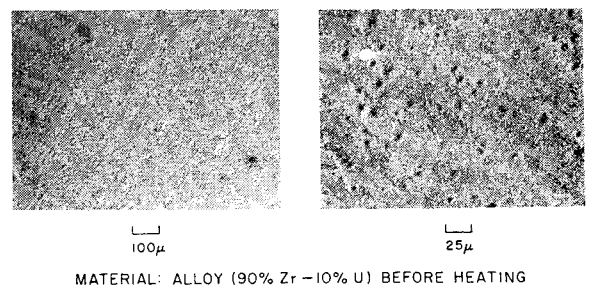

Fig. 4 Zirconium-10% uranium alloy.

Table 2 Simulation of *a* trajectory

Time, sec	Pressure, in., Hg	Flux, Btu/ft²-sec $\dot{q}_s$	Flux, Btu/ft²-sec $\bar{q}_i$	Temperature, °R Alloy	Alloy	Hydride	Hydride
300	...	45	68	2255	2330	2255	2200
100	0.04	90	145	2530	2690	2330	2240
100	0.24	200	300	3100	3190	2580	2510
100	1.40	340	510	3390	3500	3030	3010
100	2.40	140	210	2740	2800	2310	2320

and 5. The alloy has a very fine crystal structure, without characteristic markings. The hydrided material shows very large, banded crystals, characteristic of hydrides containing more than 1.6 atoms of hydrogen per atom of zirconium.

The alloy was easily cut and drilled by conventional cutting tools. The hydride, being hard and brittle, was cut with a wet carborundum wheel and drilled by a supersonic drill, as mentioned previously. The filings of hydrided material were pyrophoric; the alloy did not appear to be so.

Once the furnace was calibrated, the sample, resting on a zirconia column, was positioned in the exact focus by means of a jig. The pressure was then adjusted to correspond to the first step of the trajectory that was to be simulated. The proper flux was assured by a corresponding setting of the diaphragm. The arc was then lit and exposure was begun by using the dowser. Changes from one level to the next were made as rapidly as possible by adjusting a bleeder valve and the diaphragm, without dowsing the arc.

Temperature readings were taken at frequent intervals and an average reading was recorded for each step. The sample was closely observed through the telescope of the micropyrometer during the run.

Metallography

Surface preparation of zirconium alloy samples is quite tricky, because it tends to smear. A number of grinding and polishing techniques were tried. The following seemed to give the best results.

The samples were mounted in cold-set plastic, about $\frac{1}{16}$-in. was ground off to remove strained material, and the resulting face was polished on 600-grit silicon carbide paper. The polish marks were removed with a chemical etch consisting of 47% nitric acid (65%), 5% hydrofluoric acid (48%), and 48% hydrogen peroxide (3%). The etching solution was applied with a cotton swab and rinsed off after 10–15 sec with distilled water. If necessary, the etching was repeated until a desired surface was obtained. The sample was then rinsed in methanol and dried with warm air. It had to be examined within 1–2 hours, since an oxide coating seemed to form overnight. Typical metallographs of the structure of the alloy and hydride as received are shown in Figs. 4 and 5.

In general, it appeared that the less the samples were worked, the better the results. The surfaces obtained by the method described were reproducible.

X-ray diffraction analyses were run on a number of early samples, but they did not seem to provide much information, primarily because the equipment used "sees" all of the sample at once and therefore produces an integrated result.

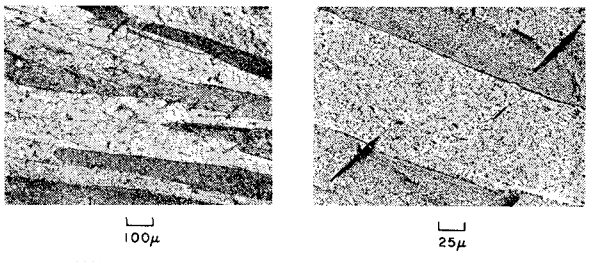

Fig. 5 Hydrided zirconium-uranium alloy.

Experimental Results

Preliminary tests of zirconium-uranium alloy were performed with cubes. On heating in air at atmospheric pressure, the unhydrided material oxidized quickly, without melting, at fluxes from 100–600 Btu/ft²-sec. The hydrided samples behaved similarly at low flux densities, oxidizing quietly and developing numerous fissures. At high flux densities, sudden eruptions occurred, resulting in the spilling of molten metal from the inside of the cube. The metal quickly solidified and became converted into an oxide. Marked cavitation inside the cubes was noted.

Simulation of *a* Trajectories

The first set of trajectories to be simulated were the *a* trajectories, corresponding to the flight path of an object having a ballistic parameter $W/C_DA = 20$ lb/psf. They are

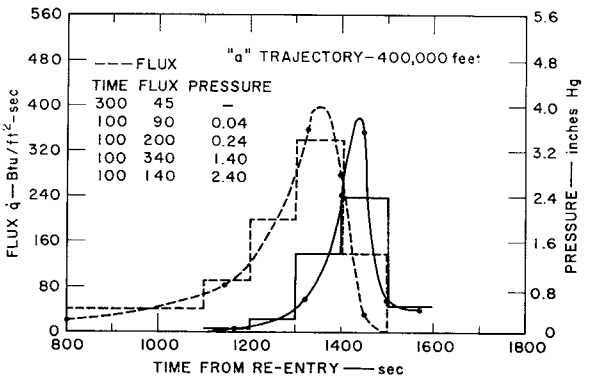

Fig. 6 Trajectory *a*; 400,000 ft.

characteristic of the conditions encountered by a fuel rod ejected from the reactor at various altitudes in a normal orientation, that is, with their long axis perpendicular to the direction of flight.

A graph of the *a* trajectory (ejection altitude 400,000 ft) and the appearance of typical samples subjected to the conditions detailed in Table 2 are shown in Figs. 6 and 7. The samples show a much larger grain structure than the material

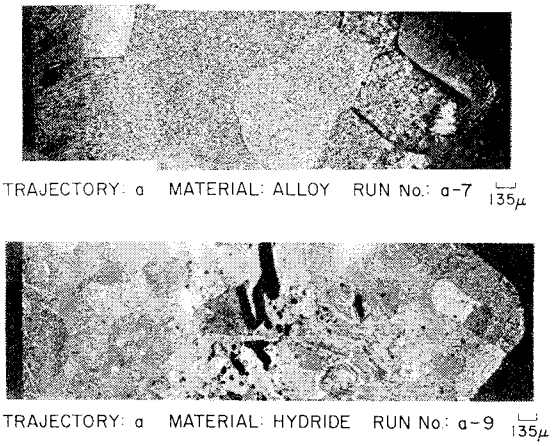

Fig. 7 Samples of material from *a* trajectory.

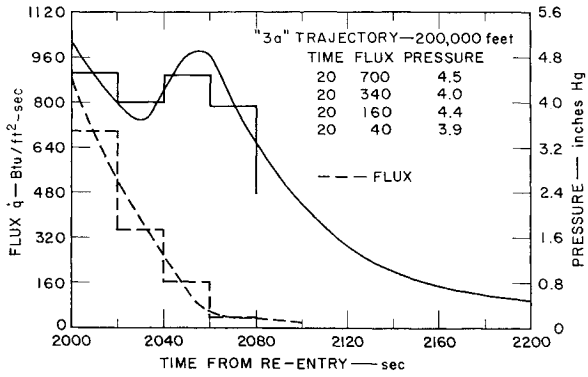

Fig. 8 Trajectory 3*a*; 200,000 ft.

and a characteristic columnar structure on the oxidized surface. The hydrided sample shows no traces of the original structure and is honeycombed with voids. There is no evidence of oxidation.

In Table 2 and in all of the tables to follow, $\bar{q}_s$ denotes the average stagnation flux calculated for the interval in question (in the present case shown in Fig. 6), and $\bar{q}_i$ denotes the actual (with some exceptions to be noted in the following) input flux, increased to compensate for the difference between aerodynamic heating and radiative heating of only one surface, as discussed previously.

The 1*a* trajectory (ejection at 300,000 ft) was run similarly. The samples were quite similar in appearance to the previous ones: again there were large crystals with a martensitic fine structure, columnar crystals around the edges of the sample, and the characteristic voids in the hydride sample. There seemed to be a thin oxide coating around the periphery of both samples.

The 2*a* trajectory (ejection at 250,000 ft) was also run at high flux. Again there was the same characteristic behavior of the samples: there was no melting, the temperature attained by the hydrided sample was about 100°C lower than for the alloy, and there was a fairly rapid dehydrogenation evidenced at times by a movement of the sample on its pedestal. The photomicrographs showed very little change in the appearance of the alloy, only dehydrogenation of the hydrided sample.

Beginning with the 3*a* trajectory, the shape of the heat pulse changes. Instead of a maximum-type curve, we now have a decaying pulse, starting at high values and then dropping off

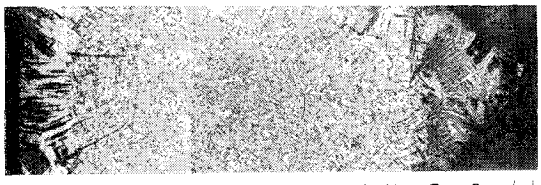

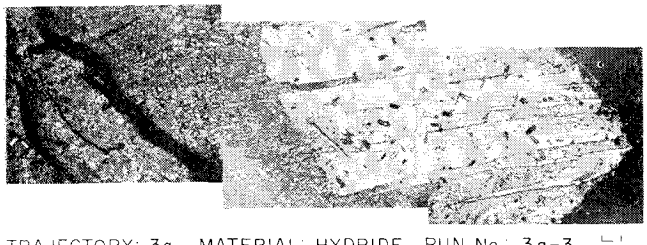

Fig. 9 Samples of material from 3*a* trajectory at average stagnation flux.

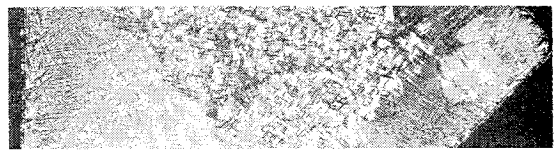

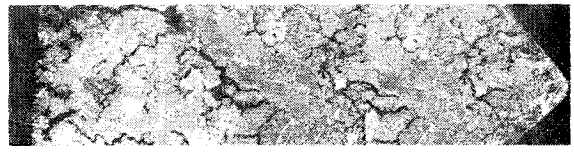

Fig. 10 Samples of material from 3*a* trajectory at increased flux.

rapidly. The total integrated heat content, represented by the area under the curve, decreases very rapidly as ejection occurs at successively lower altitudes. The trajectory and photomicrographs of the samples are shown in Figs. 8, 9, and 10. Figure 9 shows the appearance of a run made at $\bar{q}_s$. The hydride sample (no. 3*a*-3) is of particular interest, as it shows a transition of hydrided to unhydrided material. The regular sample, run at the higher-flux level, reached a temperature almost 200°C higher. The alloy sample resembled the one run at lower-flux levels, showing only a thin, adhering oxide layer and no profound changes in the metal. The hydrided sample showed a pattern of fine fissures, rather uniformly distributed through the sample (Fig. 10). Data are shown in Table 3.

The 4*a* trajectory has an even shorter history of exposure, i.e., only 60 sec. Starting out with a strong heat pulse at relatively high gas pressures, i.e., almost an atmosphere, resulted in a distinct oxide layer on the outside of the alloy sample, followed by a layer of columnar crystals. The interior of the sample showed little change. The hydrided sample lost hydrogen very rapidly under these conditions and showed a regular pattern of large fissures. It is noteworthy that no oxide was formed on this sample, suggesting that the evolving hydrogen consumes all of the oxygen available at the surface of the sample.

During several of the hydride runs simulating 3*a* and 4*a* trajectories, transient accumulation of moisture was noticed on the walls of the confining vessel. This suggests a catalytic oxidation of hydrogen at the metal surface, at least of these higher pressures.

Simulation of *b* Trajectories

The heating and pressure histories of fuel elements entering the atmosphere in an axial alignment differ considerably from those of elements entering in a crossflow position. The

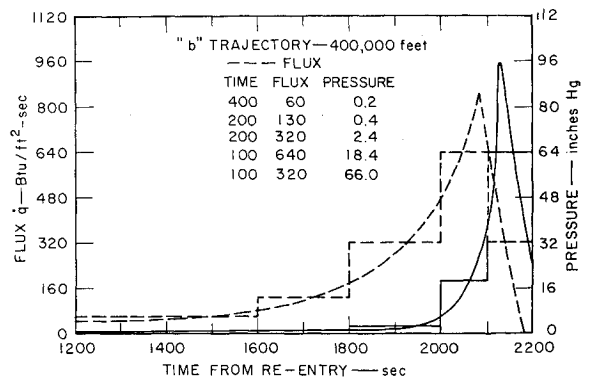

Fig. 11 Trajectory *b*; 400,000 ft.

Table 3 Simulation of 3*a* trajectory

Time, sec	Pressure, in., Hg	Flux, Btu/ft²-sec $\dot{q}_s$	Flux, Btu/ft²-sec $\dot{q}_i$	Temperature, °R Alloy 3*a*-2	Alloy 3*a*-5	Alloy 3*a*-6	Hydride 3*a*-3[a]	Hydride 3*a*-7	Hydride 3*a*-8
20	4.5	700	900	3500	3480	3895	3140	3535	3515
20	4.0	340	510	3320	2960	3010	3010	2060	2995
20	4.4	160	240	2545	2260	2420	2400	2385	2400
20	3.9	40	60	2420	2110	2110	2310	2145	2185

[a] Run at $\dot{q}_s$.

Table 4 Simulation of *b* trajectory

Time, sec	Pressure, in., Hg	Flux, Btu/ft²-sec $\dot{q}_s$	Flux, Btu/ft²-sec $\dot{q}_i$	Temperature, °R Alloy *b*-5	Alloy *b*-6	Hydride *b*-7	Hydride *b*-8
400	0.2	60	90	2470	2510	2530	2470
200	0.4	130	195	2650	2650	2635	2615
200	2.4	320	480	3085	3155	3335	3245
100	18.4	640	900	3640	3695	3820	3840
100	66.0	320	480	3085	3155	3065	3140

Table 5 Simulation of 2*b* trajectory

Time, sec	Pressure, in., Hg	Flux, Btu/ft²-sec $\dot{q}_s$	Flux, Btu/ft²-sec $\dot{q}_i$	Temperature, °R Alloy 2*b*-1	Alloy 2*b*-2	Hydride 2*b*-4
50	1.2	245	360	2565	2510	2290
50	8.8	450	675	3280	3320	2940
50	36.8	720	900	3515	3590	3550
50	62.0	400	600	3190	3210	3010

much higher value of the ballistic parameter W/C_DA resulted not only in a higher heat flux but also in much higher stagnation pressures experienced by these elements. This in turn was conducive to more rapid oxidation of the samples; and since the resulting zirconium dioxide is a very refractory material, its presence counteracted the effects of the higher heat flux and prevented melting of the specimens.

Since above-atmospheric pressures were encountered in simulation of the *b* trajectory (Fig. 11), the high-pressure reaction chamber (described earlier) was used. The alloy sample (Fig. 12) showed curiously little change other than a growth of grain size. A heavy oxide coating that was apparently cohesive enough to prevent further damage was in evidence. The hydrided material, on the other hand, was heavily oxidized, both externally and internally. This was undoubtedly due to the many fissures that developed while dehydriding, which made rapid oxidation possible. Data for this run are shown in Table 4.

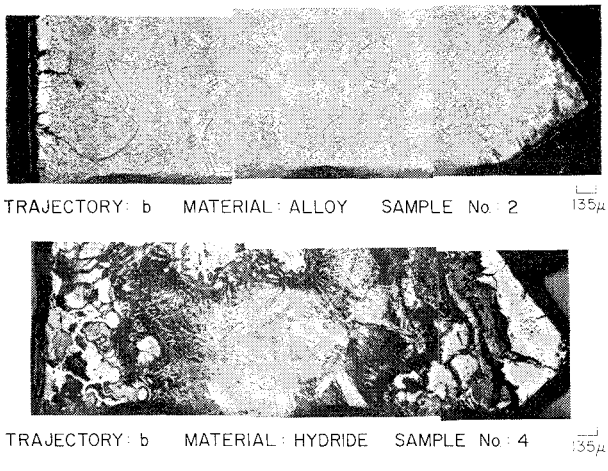

Fig. 12 Samples of material from *jb* traectory.

The discrepancy in appearance of hydrided samples representing the 4*a* and *b* trajectories, both of which were mechanically weakened by the extensive fissuring, appears to be primarily due to the duration of the run. The longer time available on the *b* trajectory permitted heavy oxidation of the dehydrided sample.

The 1*b* trajectory was simulated with both calculated $\dot{q}_s$ flux and 50% excess. An increase of temperature of about 200°R resulted from this change. The temperature reached at maximum flux was 3800°R, sufficient to cause melting of the front surface of the alloy sample. The sample was also heavily oxidized. The hydrided sample, though badly broken up and oxidized, did not show any evidence of melting, having reached a maximum temperature of only 3680°R.

The 2*b* trajectory shown in Fig. 13 is characterized both by a very high peak flux and pressure and by a relatively short duration of the heat pulse (about 200 sec). The photomicrograph of the alloy sample shows considerable oxidation and that of the hydrided sample shows evidence of violent de-

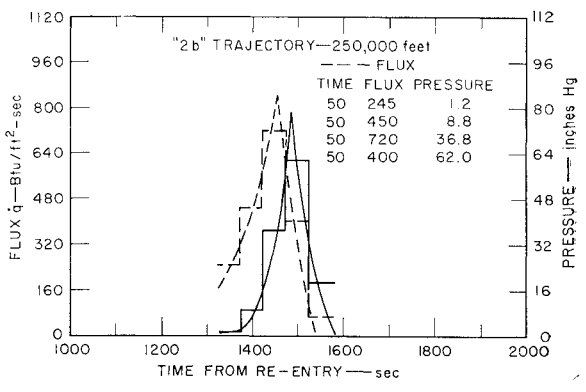

Fig. 13 Trajectory 2*b*; 250,000 ft.

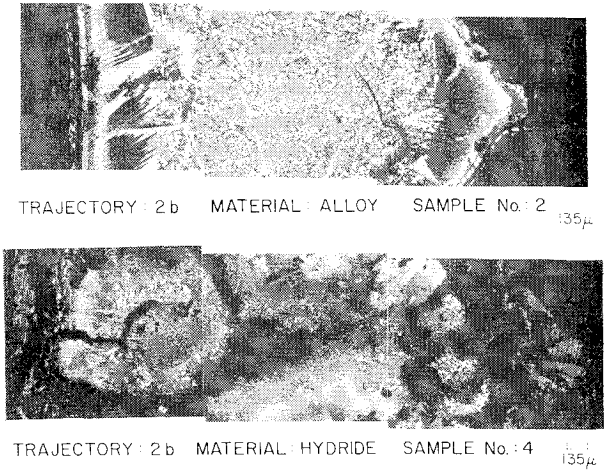

Fig. 14 Samples of material from 2*b* trajectory.

gassing, such as large cavities, but only a moderate amount of oxidation (Fig. 14). The samples did not melt; Table 5 gives details of conditions.

The 3*b* trajectory is characterized by relatively high air pressures and moderately high flux levels, as well as a short over-all duration. This combination of factors produced very little change in the alloy sample beyond a thin oxide layer and a layer of columnar crystals. Even the hydrided sample showed only moderate disruption, though it is pocketed by small voids and fissures. There was remarkably little oxidation.

Discussion

A considerable amount of evidence has been accumulated which suggests that hydrided zirconium-uranium alloy fuel elements will not melt and/or ablate when subjected to flux and pressure conditions simulating a variety of possible re-entry conditions. The conditions encountered seem to be right on the borderline; it is possible that in actual practice slightly higher fluxes would be produced and ablation would result. On the other hand, some of the assumptions made in the calculations of heating rates, such as cold-wall heat transfer, tend to give higher results than might be expected. In any case, it appears that there is not a sufficient safety factor (say, of the order of 2) to assure destruction of these elements by incineration.

It must be realized that the particular experimental approach taken deliberately neglected the effect of aerodynamic shear forces present under actual conditions. An evaluation of the possible effect of these forces, even from experiments under dynamic conditions such as a plasma jet stream, is very difficult because of the magnitude of the extrapolation required, i.e., from approximately sonic conditions to Mach 25 or 30.

References

[1] Philbin, E. J., "Re-entry and disposal for NAPS," General Dynamics/Astronautics, Rept. AE 63-0011 (1963).

[2] Sparrow, E. M., Albers, L. N., and Eckert, E. R. G., "Radiation characteristics of cylindrical enclosures, J. Heat Transfer **84**, 73–81 (1962).